Thermal conductivity of water: Molecular dynamics and generalized hydrodynamics results

Davide Bertolini
Istituto di Fisica Atomica e Molecolare del CNR, Via del Giardino 7, I-56127 Pisa, Italy

Alessandro Tani*
Dipartimento di Chimica e Chimica Industriale, Universitá di Pisa, Via Risorgimento 35, I-56126 Pisa, Italy
(Received 18 February 1997)

Equilibrium molecular dynamics simulations have been carried out in the microcanonical ensemble at 300 and 255 K on the extended simple point charge (SPC/E) model of water [Berendsen *et al.*, J. Phys. Chem. **91**, 6269 (1987)]. In addition to a number of static and dynamic properties, thermal conductivity λ has been calculated via Green-Kubo integration of the heat current time correlation functions (CF's) in the atomic and molecular formalism, at wave number $k=0$. The calculated values (0.67 ± 0.04 W/mK at 300 K and 0.52 ±0.03 W/mK at 255 K) are in good agreement with the experimental data (0.61 W/mK at 300 K and 0.49 W/mK at 255 K). A negative long-time tail of the heat current CF, more apparent at 255 K, is responsible for the anomalous decrease of λ with temperature. An analysis of the dynamical modes contributing to λ has shown that its value is due to two low-frequency exponential-like modes, a faster collisional mode, with positive contribution, and a slower one, which determines the negative long-time tail. A comparison of the molecular and atomic spectra of the heat current CF has suggested that higher-frequency modes should not contribute to λ in this temperature range. Generalized thermal diffusivity $D_T(k)$ decreases as a function of k, after an initial minor increase at $k=k_{\min}$. The k dependence of the generalized thermodynamic properties has been calculated in the atomic and molecular formalisms. The observed differences have been traced back to *intramolecular* or *intermolecular* rotational effects and related to the partial structure functions. Finally, from the results we calculated it appears that the SPC/E model gives results in better agreement with experimental data than the transferable intermolecular potential with four points TIP4P water model [Jorgensen *et al.*, J. Chem. Phys. **79**, 926 (1983)], with a larger improvement for, e.g., diffusion, viscosities, and dielectric properties and a smaller one for thermal conductivity. The SPC/E model shares, to a smaller extent, the insufficient slowing down of dynamics at low temperature already found for the TIP4P water model. [S1063-651X(97)06009-1]

PACS number(s): 61.20.Ja, 61.25.Em, 66.60.+a, 67.55.Fa

I. INTRODUCTION

In two recent papers [1,2] some collective dynamical properties of liquid water, modeled by the transferable intermolecular potential with four points TIP4P [3] potential, have been computed by molecular dynamics (MD) simulation and analyzed in the framework of generalized hydrodynamics. In particular, generalized viscosity and rigidity moduli have been studied in [2], where the contribution to these properties of the different dynamical modes of water (O–O–O bending, 8–10 THz, stretching, or cage, 45–50 THz, and librational modes 90–170 THz) has also been obtained. This has allowed illustration of the prominent role of the cage mode in determining viscosity and rigidity moduli, while the librational mode contribution to rigidity moduli is minor and that to viscosity negligible.

In this paper we extend this approach to the study of generalized thermal conductivity λ, also to analyze the contribution of the different dynamical modes to this property. This is done by calculating the time correlation function (CF) of the energy flux as well as the density-density, energy-density, and energy-energy CF's at a number of k values. The latter three functions are the key ingredients to the generalized hydrodynamics theory. Further, the results obtained with the extended simple point charge SPC/E [4] model will be compared to that relevant to the TIP4P model. The latter performs well for a number of equilibrium and dynamic properties at ambient temperature, but its behavior in the supercooled region as far as the above mentioned collective dynamical properties is concerned is still to be determined.

When generalized hydrodynamics is applied to molecular liquids, a ''molecular'' or an ''atomic'' formalism can be adopted. In the molecular formalism a single phase factor is employed for each molecule, with the coordinate of the center of mass, whereas in the atomic one each atom yields its own contribution to the computed property, modulated by its own phase factor. In the $k\rightarrow0$ limit, both formalisms lead to the same results, however, the k dependence of the results can be significantly different. Both these approaches will be employed here to calculate various generalized thermodynamic properties, namely, constant pressure and volume heat capacity, $c_P(k)$ and $c_V(k)$, thermal expansivity $\alpha(k)$, and enthalpy per molecule, $h(k)$. Moreover, intramolecular (self) contributions to these properties will be computed to gain further insight, e.g., into the relative effects of rotational and translational motions.

This paper is organized as follows. A brief outline of the theoretical approach used to analyze the simulation results is given in Sec. II. The MD results of λ are presented in Sec. III A and compared with the experimental data; in Sec. III B the dynamical modes contributing to λ are discussed and Sec. III C extends this analysis to finite k. Generalized ther-

*Author to whom correspondence should be addressed.

modynamics parameters are reported and discussed in Sec. III D and the very-high-k dynamics in Sec. III E. The main results and conclusions are summarized in Sec. IV.

II. THEORETICAL BACKGROUND

The approach adopted in this paper has been described in detail elsewhere [1,2,5] so we only recall here the results and relations required for the discussion in the following. The theory is based on a set of time correlation functions $F_{ij}(k,t)$, where the indices $i,j(=1-5)$ label density, longitudinal velocity, energy, stress tensor, and longitudinal heat flux, respectively. A set of orthonormal linear combinations of the CF's $F_{ij}(k,t)$, $G_{ij}(k,t)$ is also introduced which facilitates theoretical analysis and interpretation of results.

Thermal conductivity at $k=0$ can be obtained from the Green-Kubo relation

$$\lambda^{(\mathrm{at.},m)}=\frac{\rho M}{k_B T^2}\int_0^\infty F_{55}^{(\mathrm{at.},m)}(0,t)dt \tag{2.1}$$

for both atomic (at.) and molecular (m) expressions of $F_{55}(0,t)$. This relation, however, cannot simply be extended to $k>0$ to calculate a generalized thermal conductivity, because of the conservation law that links $F_{55}(k,t)$ to $F_{33}(k,t)$ [2,5],

$$F_{55}(k,t)=-\frac{1}{k^2}\frac{\partial^2 F_{33}(k,t)}{\partial t^2}, \tag{2.2}$$

which would lead to a zero value of $\lambda(k)$, via an integral like Eq. (2.1).

Rather, one can obtain $\lambda(k)$ from the generalized thermal diffusivity $D_T(k)$ through $G_{33}(k,t)$,

$$G_{33}(k,t)=\frac{\left[\left(\frac{V_{13}(k)}{V_{11}(k)}\right)^2 F_{11}(k,t)-2\frac{V_{13}(k)}{V_{11}(k)}F_{13}(k,t)+F_{33}(k,t)\right]}{\left(V_{33}(k)-\frac{V_{13}(k)^2}{V_{11}(k)}\right)}, \tag{2.3}$$

where $V_{ij}(k)\equiv F_{ij}(k,0)$, defining

$$D_T(k)=\lim_{z\to 0}\widetilde{D}_T(k,z)=\lim_{z\to 0}\frac{\widetilde{N}_q(k,z)}{k^2}\cong\lim_{z\to 0}\frac{1}{k^2\widetilde{G}_{33}(k,z)}, \tag{2.4}$$

as, from generalized hydrodynamics,

$$\frac{1}{\widetilde{G}_{33}(k,z)}\cong z+\widetilde{N}_q(k,z)=z+f_{Tq}^2(k)\widetilde{n}_q(k,z). \tag{2.5}$$

In Eq. (2.5) $\widetilde{n}_q(k,z)$ is the spectrum of the memory kernel of $G_{33}(k,t)$ and $f_{Tq}(k)$ is the corresponding characteristic frequency [1].

Alternatively, one can use $G_{55}(k,t)$, defined as

$$G_{55}(k,t)=\frac{\left[\left(\frac{V_{25}(k)}{V_{22}(k)}\right)^2 F_{22}(k,t)-2\frac{V_{25}(k)}{V_{22}(k)}F_{25}(k,t)+F_{55}(k,t)\right]}{\left(V_{55}(k)-\frac{V_{25}(k)^2}{V_{22}(k)}\right)}, \tag{2.6}$$

which is related to $\widetilde{N}_q(k,z)$ by

$$\widetilde{G}_{55}(k,z)\cong\frac{\widetilde{N}_q(k,z)}{f_{Tq}^2(k)}\frac{z}{z+\widetilde{N}_q(k,z)}, \tag{2.7}$$

so that

$$\widetilde{D}_T(k,z)\cong\frac{f_{Tq}^2(k)}{k^2}\frac{z\widetilde{G}_{55}(k,z)}{z-f_{Tq}^2(k)\widetilde{G}_{55}(k,z)}. \tag{2.8}$$

It should be noted that this route to $\lambda(k)$ is not independent from the other and that Eqs. (2.4) and (2.5) and Eqs. (2.7) and (2.8) hold only when $\gamma=c_P/c_V=1$ and the coupling between stress tensor and heat flux can be neglected. These conditions are well satisfied in water at least up to $k=1$ Å^{-1}. More general expressions can be found in Ref. [1]. Hence a generalized thermal conductivity can be obtained from

$$\widetilde{\lambda}(k,z)\equiv\rho c_V(k)\widetilde{D}_T(k,z). \tag{2.9}$$

At $k=0$ constant volume heat capacity can be obtained, in a ''microcanonical'' MD, from the fluctuations of kinetic energy [6]:

$$c_V=\frac{3R}{1-3(N/T^2)\langle\Delta T^2\rangle}. \tag{2.10}$$

Moreover, as in [1], generalized enthalpy $h(k)$, constant volume and pressure heat capacity, $c_V(k)$ and $c_P(k)$, their ratio $\gamma(k)$, and the thermal expansivity $\alpha(k)$ can be obtained from the initial values $V_{ij}(k)$ of the $F_{ij}(k,t)$ according to the following relations [5,7], derived for a simple atomic fluid:

$$\alpha(k)=\frac{h(k)V_{11}(k)-V_{13}(k)}{k_B T^2}, \tag{2.11}$$

$$c_V(k)=\frac{V_{33}(k)-V_{13}(k)^2/V_{11}(k)}{k_B T^2}, \tag{2.12}$$

$$\gamma(k)=1+\frac{[h(k)V_{11}(k)-V_{13}(k)]^2}{V_{11}(k)[V_{33}(k)-V_{13}(k)^2/V_{11}(k)]}, \tag{2.13}$$

where

$$h(k)=\frac{V_{25}(k)}{V_{22}(k)}=\frac{V_{34}(k)}{V_{22}(k)}. \tag{2.14}$$

To understand the k dependence of these properties, it is necessary to calculate the self (S) contribution to the coefficients $V_{ij}(k)$ that appear in Eqs. (2.11)–(2.14).

For the density-density correlation one has

$$V_{11}^{(S,m)}=1,$$

$$V_{11}^{(S,at)}(k)=2\frac{m_{\mathrm{H}}^2}{M^2}[1+j_0(kr_{\mathrm{HH}})]+\frac{m_{\mathrm{O}}^2}{M^2}+4\frac{m_{\mathrm{H}}m_{\mathrm{O}}}{M^2}j_0(kr_{\mathrm{OH}}). \tag{2.15}$$

For the density energy

$$V_{13}^{(S,m)}=2\langle E_{\mathrm{H}}\rangle+\langle E_{\mathrm{O}}\rangle,$$

$$V_{13}^{(S,at)}(k)=2\frac{m_{\mathrm{H}}}{M}\langle E_{\mathrm{H}}\rangle[1+j_0(kr_{\mathrm{HH}})]+\frac{m_{\mathrm{O}}}{M}\langle E_{\mathrm{O}}\rangle+2\left(\frac{m_{\mathrm{O}}}{M}\langle E_{\mathrm{H}}\rangle+\frac{m_{\mathrm{H}}}{M}\langle E_{\mathrm{O}}\rangle\right)j_0(kr_{\mathrm{OH}}), \tag{2.16}$$

and for the energy energy

$$V_{33}^{(S,m)}=A+A_{\mathrm{HH}}+A_{\mathrm{OH}},$$

$$V_{33}^{(S,at)}(k)=A+A_{\mathrm{HH}}j_0(kr_{\mathrm{HH}})+A_{\mathrm{OH}}j_0(kr_{\mathrm{OH}}), \tag{2.17}$$

where

$$A=2[\langle E_{\mathrm{H}}^2\rangle-\langle E_{\mathrm{H}}\rangle^2]+\langle E_{\mathrm{O}}^2\rangle-\langle E_{\mathrm{O}}\rangle^2,$$

$$A_{\mathrm{HH}}=2[\langle E_{\mathrm{H}_1}E_{\mathrm{H}_2}\rangle-\langle E_{\mathrm{H}_1}\rangle\langle E_{\mathrm{H}_2}\rangle],$$

$$A_{\mathrm{OH}}=4[\langle E_{\mathrm{H}}E_{\mathrm{O}}\rangle-\langle E_{\mathrm{H}}\rangle\langle E_{\mathrm{O}}\rangle]. \tag{2.18}$$

For the longitudinal current we obtain

$$V_{22}^{(S,m)}=\frac{k_BT}{M},$$

$$V_{22}^{(S,at)}(k)=\frac{k_BT}{M}[B+B_{\mathrm{HH}}j_0(kr_{\mathrm{HH}})+C_{\mathrm{HH}}j_2(kr_{\mathrm{HH}})+B_{\mathrm{OH}}j_0(kr_{\mathrm{OH}})+C_{\mathrm{OH}}j_2(kr_{\mathrm{OH}})]. \tag{2.19}$$

The coefficients B, B_{HH}, C_{HH}, B_{OH}, and C_{OH} can be obtained as described in Refs. [8, 9]. Analogously, one has for the amplitude of the coupling between energy and longitudinal stress, or longitudinal current-heat flux, which are equivalent as $F_{34}(k,t)=F_{25}(k,t)$,

$$V_{25}^{(S,m)}=\left\langle\left(\frac{\mathbf{k}}{k}\cdot\mathbf{v}\right)^2E\right\rangle-\left\langle\left(\frac{\mathbf{k}}{k}\cdot\mathbf{v}\right)^2\right\rangle\langle E\rangle,$$

$$V_{25}^{(S,at)}(k)=D_{\mathrm{H}}+D_{\mathrm{O}}+D_{\mathrm{HH}}(k)+D_{\mathrm{OH}}(k), \tag{2.20}$$

where

$$D_{\mathrm{H}}=2\frac{m_{\mathrm{H}}}{M}\left[\left\langle\left(\frac{\mathbf{k}}{k}\cdot\mathbf{v}_{\mathrm{H}}\right)^2E_{\mathrm{H}}\right\rangle-\left\langle\left(\frac{\mathbf{k}}{k}\cdot\mathbf{v}_{\mathrm{H}}\right)^2\right\rangle\langle E_{\mathrm{H}}\rangle\right],$$

$$D_{\mathrm{O}}=\frac{m_{\mathrm{O}}}{M}\left[\left\langle\left(\frac{\mathbf{k}}{k}\cdot\mathbf{v}_{\mathrm{O}}\right)^2E_{\mathrm{O}}\right\rangle-\left\langle\left(\frac{\mathbf{k}}{k}\cdot\mathbf{v}_{\mathrm{O}}\right)^2\right\rangle\langle E_{\mathrm{O}}\rangle\right], \tag{2.21}$$

$$D_{\mathrm{HH}}(k)=\frac{m_{\mathrm{H}}}{M}\left\langle\left[E_{\mathrm{H}_1}\left(\frac{\mathbf{k}}{k}\cdot\mathbf{v}_{\mathrm{H}_2}\right)^2+E_{\mathrm{H}_2}\left(\frac{\mathbf{k}}{k}\cdot\mathbf{v}_{\mathrm{H}}\right)^2\right]\times\cos[\mathbf{k}\cdot(\mathbf{r}_{\mathrm{H}_1}-\mathbf{r}_{\mathrm{H}_2})]\right\rangle,$$

$$D_{\mathrm{OH}}(k)=2\left\langle\left[\frac{m_{\mathrm{H}}}{M}E_{\mathrm{O}}\left(\frac{\mathbf{k}}{k}\cdot\mathbf{v}_{\mathrm{H}}\right)^2+\frac{m_{\mathrm{O}}}{M}E_{\mathrm{H}}\left(\frac{\mathbf{k}}{k}\cdot\mathbf{v}_{\mathrm{O}}\right)^2\right]\times\cos[\mathbf{k}\cdot(\mathbf{r}_{\mathrm{O}}-\mathbf{r}_{\mathrm{H}})]\right\rangle.$$

In Eqs. (2.15)–(2.21) j_0 and j_2 are the spherical Bessel functions of order 0 and 2, E_j is total energy of atom j, and $E=\Sigma_jE_j$ total energy of the molecule. A result analogous to Eq. (2.19) can be derived from Eq. (2.21) and we omit details here.

Notice that forces, which give by far the largest contribution to $F_{34}(k,t)$ at $k=0$, are absent in Eq. (2.21), while they are the dominant term of the collective or cross (C) part. The latter, in the molecular formalism, is defined by

$$V_{34}^{(C,m)}(k)=\left\langle\sum_{\alpha\neq\beta}\left(\frac{\mathbf{k}}{k}\cdot\mathbf{v}_\alpha\right)^2E_\beta\cos[\mathbf{k}\cdot(\mathbf{r}_\alpha-\mathbf{r}_\beta)]+\frac{1}{kM}\left(\frac{\mathbf{k}}{k}\cdot\mathbf{F}_\alpha\right)E_\beta\sin[\mathbf{k}\cdot(\mathbf{r}_\alpha-\mathbf{r}_\beta)]\right\rangle, \tag{2.22}$$

where E_β (<0) is total energy of molecule β and $\mathbf{F}_\alpha$ the total force acting on molecule α. The corresponding atomic expression contains terms which are analogous to that of Eq. (2.22), but also, as a new feature, terms related to different atoms of different molecules, which are dominated by rotational motions. This difference is at the basis of the different k dependence of generalized enthalpy $h(k)=V_{34}/V_{22}$ observed with the two formalisms, see Sec. III D.

The contribution of the various dynamical modes of water to the coefficients of Eqs. (2.11)–(2.13) is determined by an analysis of the time dependence of the time correlation functions $F_{ij}(k,t)$, which, as in Ref. [1], are fitted with combinations of complex exponentials. This can be done up to $k\approx10\ \text{Å}^{-1}$, when the time dependence becomes Gaussian-like. In this limit ($k\to\infty$), we adopted the approach used by Alley and Alder [10], by averaging over a Maxwellian distribution of velocities. We obtain for the density-density and density-energy CF's

$$F_{11}^{(m)}(k\to\infty,t)=\exp(-at^2),$$

$$F_{11}^{(at)}(k\to\infty,t)=2\frac{m_{\rm H}^2}{M^2}\exp(-aA_{R\rm H}t^2)+\frac{m_{\rm O}^2}{M^2}\exp(-aA_{R\rm O}t^2), \quad (2.23)$$

$$F_{13}^{(m)}(k\to\infty,t)=V_{13}^{(S,m)}(1-\gamma_{13}^{(m)}t^2)\exp(-at^2),$$

$$\frac{F_{13}^{(at)}(k\to\infty,t)}{V_{13}^{(S,\rm at.)}(\infty)}=\alpha_{13}(1-\gamma_{13\rm H}^{(at)}t^2)\exp(-aA_{R\rm H}t^2)+(1-\alpha_{13})\times(1-\gamma_{13\rm O}^{(at)}t^2)\exp(-aA_{R\rm O}t^2), \quad (2.24)$$

where

$$\gamma_{13}^{(m)}=\frac{k_BT}{V_{13}^{(S,m)}}a,$$

$$\gamma_{13\rm H}^{(at)}=\frac{k_BT}{\langle E_{\rm H}\rangle}\frac{m_{\rm H}}{M}A_{R\rm H}a, \quad (2.25)$$

$$\alpha_{13}=2\frac{m_{\rm H}\langle E_{\rm H}\rangle}{MV_{13}^{(S,\rm at.)}(\infty)}.$$

$a=(k_BT/M)k^2/2$ and $A_{R\rm H}=9.564$, $A_{R\rm O}=1.0545$ are constants depending on the geometrical parameters of the models and on the moments of inertia of the molecule. Finally, we have for the energy-energy CF

$$F_{33}^{(m)}(k\to\infty,t)=V_{33}^{(S,m)}(1-\gamma_{33}^{(m)}t^2+\delta_{33}^{(m)}t^4)\exp(-at^2),$$

$$\frac{F_{33}^{(at)}(\infty,t)}{V_{33}(\infty)^{(S,\rm at.)}}=\alpha_{33}(1-\gamma_{33\rm H}^{(at)}t^2+\delta_{33\rm H}^{(at)}t^4)\exp(-aA_{R\rm H}t^2)+(1-\alpha_{33})(1-\gamma_{33\rm O}^{(at)}t^2+\delta_{33\rm O}^{(at)}t^4)\times\exp(-aA_{R\rm O}t^2), \quad (2.26)$$

where

$$\gamma_{33}^{(m)}=\frac{3}{2}\frac{\langle E\rangle k_BT}{V_{33}^{(S,m)}}a,$$

$$\delta_{33}^{(m)}=\frac{9}{4}\frac{(k_BT)^2}{V_{33}^{(S,m)}}a^2, \quad (2.27)$$

and

$$\gamma_{33\rm H}^{(at)}=\frac{\langle E_{\rm H}\rangle(k_BT)}{V_{33}(\infty)^{(S,at)}}A_{R\rm H}^2a,$$

$$\delta_{33\rm H}^{(at)}=\frac{(k_BT)^2}{V_{33}^{(S,\rm at.)}}A_{R\rm H}^4a^2,$$

$$\alpha_{33}=2\frac{[\langle E_{\rm H}^2\rangle-\langle E_{\rm H}\rangle^2]}{V_{33}^{(S,\rm at.)}(\infty)}. \quad (2.28)$$

In the $k\to\infty$ limit, the other functions, $F_{22}(k,t)$, $F_{44}(k,t)$, $F_{25}(k,t)$, and $F_{55}(k,t)$, can be obtained from Eqs. (2.23) and (2.24)–(2.26) through conservation laws [5].

III. RESULTS AND DISCUSSION

The results presented below have been obtained by molecular dynamics simulation of a sample of 343 water molecules in the microcanonical ensemble. The potential adopted is the modified SPC function, usually referred to as SPC/E. This potential assumes a tetrahedral geometry for water, with an OH bond length of 1 Å. A short-range Lennard-Jones term with $\sigma=3.1656$ Å and $\varepsilon=0.65$ kJ/mol acts on the oxygen, while a charge $q=0.4238e$ is on each hydrogen, compensated by a charge $-2q$ on the oxygen. The long-range Coulombic part has been treated with the Ewald sum scheme and with a cutoff distance for the short-range interactions at half the box side. The equations of motion have been integrated with the constraint method [11] with a time step of 2 fs at 300 K and 2.5 fs at 255 K. The total time spanned after equilibration has been 700 ps at 300 K and 800 ps at 255 K.

The values of some equilibrium and dynamical properties calculated for the SPC/E model of water are collected in Table I and compared to the corresponding results for the TIP4P model from previous work [1,2] and to experimental data. The viscosity of the SPC/E water model has been obtained with the same procedure adopted in [2] for the TIP4P model. As can be seen, the overall agreement between calculated and experimental data is better for the SPC/E than for the TIP4P water model, especially at the lower temperature. In this range, we already found that the dynamics of the TIP4P water model is faster than that of real water. The SPC/E model performs well also from the point of view of static dielectric constant and its temperature dependence, which we evaluated $\varepsilon_0=78\pm9$ at 255 K and $\varepsilon_0=74\pm8$ at 300 K with runs of 800 and 700 ps, respectively. The reported uncertainty is derived from the spread of the diagonal components of the Kirkwood tensor around the average.

As in [1] the time correlation functions $F_{ij}(k,t)$ have been computed at 255 and 300 K in the atomic and molecular formalism for a number of k values, ranging from $k_{\rm min}=0.288$ Å^{-1} to a rather high value of ≈45 Å^{-1}. We directly computed all $F_{ij}(k,t)$ at finite k except $F_{55}(k,t)$ that was obtained exploiting conservation laws, Eq. (2.2). This procedure allowed us to check internal consistency of the calculation by a test of relations such as, e.g., $F_{14}(k,t)=F_{22}(k,t)=-(1/k^2)[\partial^2F_{11}(k,t)/\partial t^2]$. $F_{44}(k,t)$ and $F_{55}(k,t)$, however, have been computed directly, at $k=0$, where they can be used to obtain viscosity and thermal conductivity via Green-Kubo relations [see Eq. (2.1)]. $F_{55}(0,t)$ is the time correlation function of the heat flux vector, which has been calculated according to the definition given by Marechal and Ryckaert [20].

A. Thermal conductivity

$F_{55}(0,t)$ has been calculated for all three components of the heat flux vector and its average is shown in Fig. 1 for both temperatures and formalisms. This allowed us to estimate the error and monitor convergence, which, on the inte-

TABLE I. Calculated equilibrium (a) and dynamic (b) properties of SPC/E and TIP4P water models. Experimental data in parentheses.

(a)

T (K)	$-U$ (kJ/mol)	P (kbar)	ρ (g/cm^3)	α (10^{-4} K^{-1})	C_V (J/mol K)	ϵ_0
255	44.2(44.4)[a]	−0.04	1.00(0.995)[b]	2(−5.8)[b]	90.5(76)[c]	78(95.6)[d]
300	41.2(41.5)[a]	−0.12	0.985(0.996)[e]	5.5(2.8)[e]	82(74)[c]	74(78.3)[f]

(b)

T (K)	D (10^{-5} cm/s^2)	τ_S (ps)	τ_D (ps)	η (10^{-2} g/cm s)	η_L (10^{-2} g/cm s)	λ (W/mK)
245 TIP4P	0.6(0.25)[c]	14.5	39	2.1(8.0)[c]	7.6(25)[g]	0.35(0.45)
255 SPC/E	0.73(0.5)[c]	13.2	36.3(38)[d]	1.85(3.9)[c]	6.8(9.8)[g]	0.52(0.49)
298 TIP4P	3.7		7	0.47	1.7(3.0)[g]	
300 SPC/E	2.7(2.4)[c]	4.4	6.7(8.0)[f]	0.5(0.9)[c]	2.1(3.0)[g]	0.67(0.61)[h]

[a]Reference [12].
[b]Reference [13].
[c]Reference [15].
[d]Reference [16].
[e]Reference [14].
[f]Reference [17].
[g]Reference [18].
[h]Reference [19].

grated functions of Fig. 2 required averaging over 625 ps at 255 K and 460 ps at 300 K to maintain the error within ~10%. The thermal conductivity values we obtain ($\lambda = 0.67 \pm 0.04$ W/mK at 300 K and $\lambda = 0.52 \pm 0.03$ W/mK at 255 K) are in good agreement with the experimental data ($\lambda = 0.61$ W/mK [19] at 300 K and $\lambda = 0.49$ W/mK at 255 K). The latter value has been obtained extrapolating data measured on the saturation curve between 543 and 273 K. In the case of the TIP4P water model, the value of λ we calculated as described in [1] at 245 K (0.35 W/mK) was less good but still fair compared to the experimental data (0.45 W/mK), which suggests that λ may be less model dependent than other transport parameters, e.g., viscosity or diffusion. However, previous MD results [21] of λ calculated for the Carravetta-Clementi [22] model of water are much larger (~60%) than the experimental data at 298 K, although the temperature dependence of λ is qualitatively correct.

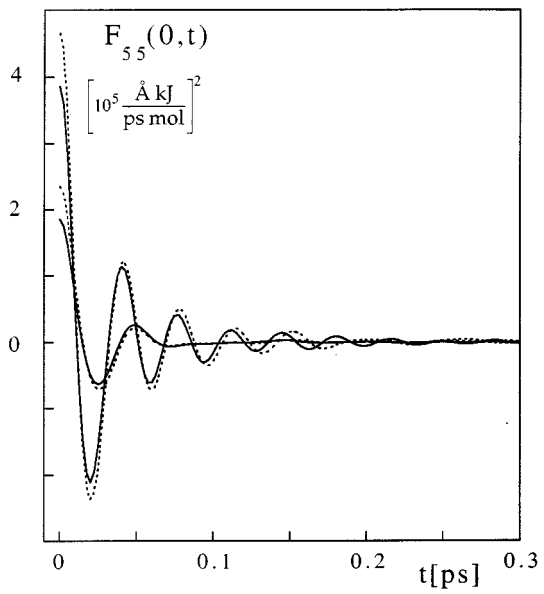

FIG. 1. Heat flux fluctuation correlation function, $F_{55}(t)$ at 255 K (full curves) and 300 K (dotted curves). The two more strongly oscillating curves are calculated in the molecular (m) formalism.

The short-time part of $F_{55}(0,t)$ (Fig. 1) is dominated by the librational dynamics, whose oscillations, with amplitude twice as large in the molecular formalism as that of the atomic functions, have essentially vanished beyond ~0.3 ps. The longer-time part, however, is very important from the point of view of the integral of $F_{55}(0,t)$ and hence of thermal conductivity, as can be seen in Fig. 2. In particular, the long-time tail, apparent in Fig. 2(a), decreases by ~40% the value of λ corresponding to the first 0.3 ps.

This long-time tail is not visible at 300 K. This different role of the long-time tail at the two temperatures can be exploited to rationalize, at least qualitwatively, the ''anomalous'' behavior of λ in water. In most liquids, alcohols for instance, thermal conductivity increases when temperature decreases, while the opposite is observed for water, more remarkably in the supercooled region. The results of Fig. 2 suggest that this is due to the long-time tail of $F_{55}(0,t)$. In fact, if the long-time tail is subtracted from $F_{55}(0,t)$, λ is larger at 255 than at 300 K, Fig. 2(b). The long-time tail of $F_{55}(0,t)$ seems to be a peculiar feature of water, presumably related to its positional and orientational correlations and their temperature dependence.

B. Dynamical modes of water and their contribution to λ

An analysis of the contribution to λ of the various dynamical modes of water, corresponding to different characteristic time scales, can be carried out through the spectra of $F_{55}(0,t)$, shown in Figs. 3 and 4. As in [1], they have been obtained by a numerical transform of the difference between the computed $F_{55}(0,t)$ and a proper fitting function, which is then added to the analytical transform of the fitting function. The most apparent feature of the spectra at both temperatures is the large high-frequency band that corresponds to libra-

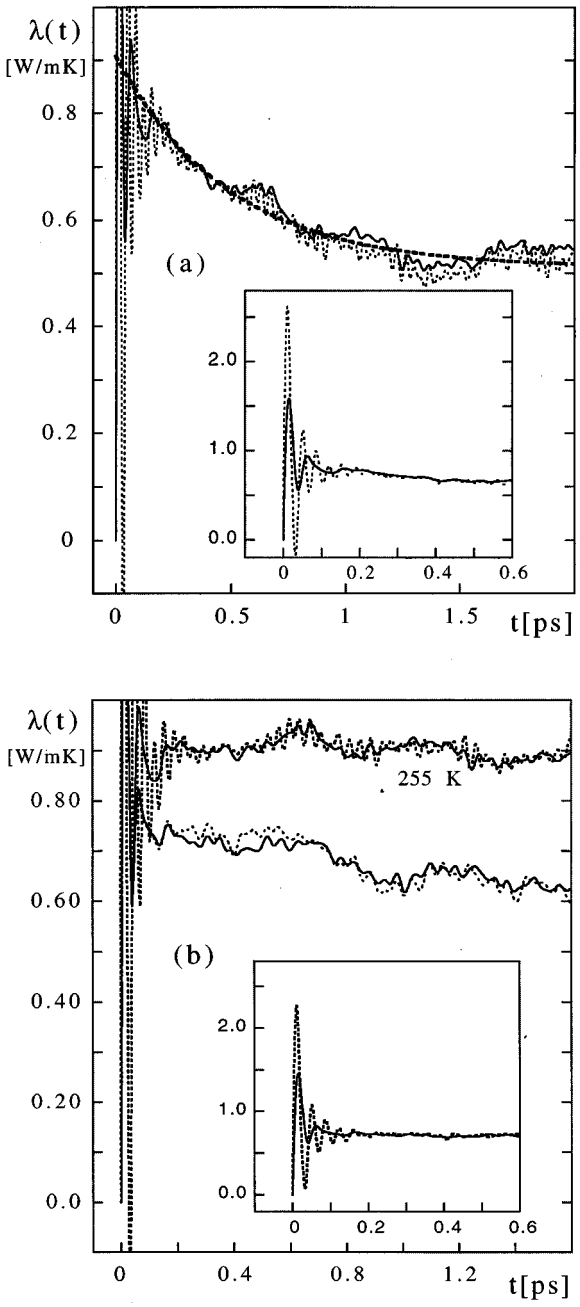

FIG. 2. Running integral of $F_{55}(t)$, i.e., $\lambda(t)$ [Eq. (2.1)], at 255 K (a) and 300 K (b). Dotted and full curves show (m) and (at) results, respectively. The insets show the short-time behavior of the integral at both temperatures. The heavy dashed curve in (a) is the fit to the long-time tail of the integral. The function labeled 255 K in (b) is the integral of (a) minus the long-time tail.

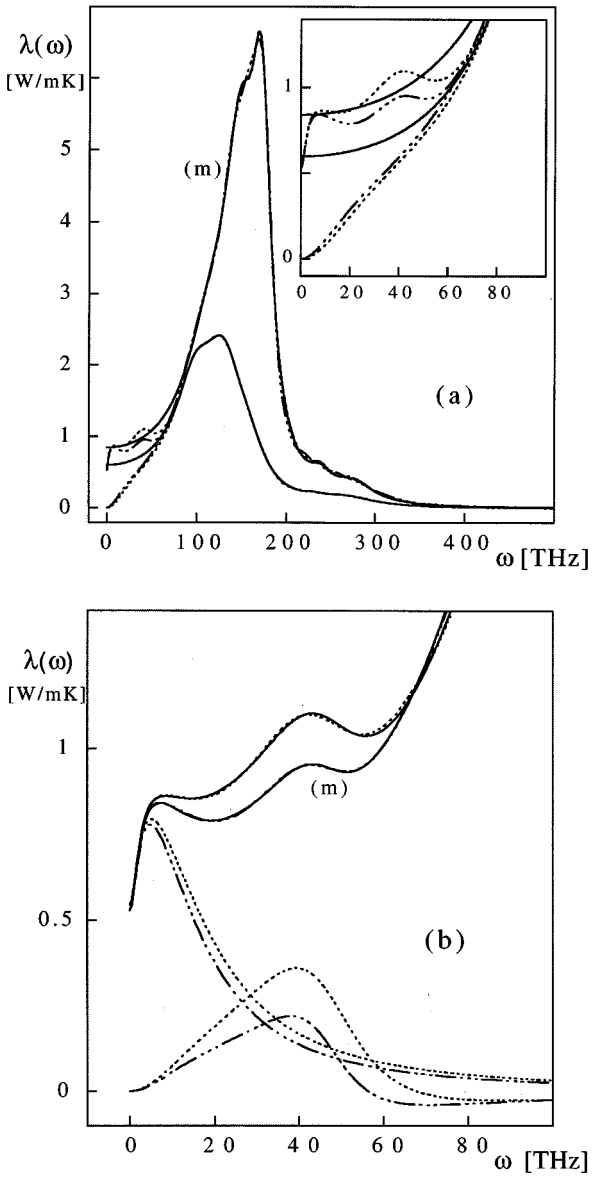

FIG. 3. (a) MD spectra of (m) (dot-dashed) and (at) (dotted) $F_{55}(t)$, in units of thermal conductivity, Eq. (2.1). The region $\omega > 80$ has been fitted with two types of functions, functions (L) [Eq. (3.2)] and (D) [Eq. (3.3)] (full curves). The former are the two upper full curves of the inset showing the low-frequency region, while the latter two vanish at $\omega = 0$. (b) Comparison of MD and fitting results with (D) functions extended to the low-frequency part of the spectrum (upper curves). The contribution of the cage mode and of the two exponentials to the fitting is also shown for both (m), dot-dashed, and atomic (at), dotted, results. $T = 255$ K.

tional motions. This band is barely visible in the spectra of $F_{44}(0,t)$ [2], indicating that the contribution of libration to viscosity is negligible. Moreover, the librational band is much larger in the molecular spectrum than in the atomic one. On the other hand, λ, i.e., the zero-frequency value of the spectrum, must be independent of the formalism adopted, and actually the whole low-frequency ($\omega < 10$ THz) part of the spectra is very similar for the molecular and atomic functions. This means that a librational contribution to thermal conductivity, presumably different for the molecular or atomic functions, should be compensated by an equal and opposite difference of the low-frequency part of the two descriptions.

This hypothesis has been tested fitting the high-frequency part of the spectra with a combination of functions, labeled L, such as [23,24]

$$f_L(t) = \exp(-\gamma_L t)\left(\cos(\omega_L t) + \frac{\gamma_L}{\omega_L}\sin(\omega_L t)\right). \quad (3.1)$$

Functions like this, with $\dot{f}_L(0) = 0$ and a transform

$$\tilde{f}_L(z)=\frac{z+2\gamma_L}{[(z+\gamma_L)^2+\omega_L^2]}, \tag{3.2}$$

give $2\gamma_L/(\gamma_L^2+\omega_L^2)$ as a contribution to $\lambda[z=0]$.

A fit of this kind with five functions, three for the librational band and two for the highest-frequency band between 200 and 350 THz, has been carried out starting from 80 THz and the results are also shown in Fig. 3(a).

As can be seen, the fit performs well for both molecular and atomic spectra in the range 80–500 THz, but the extrapolation to $\omega<80$ THz, Fig. 3(a), leads to different $\omega=0$ values, which can hardly be compensated by an equal and opposite difference of the low-frequency parts, with physically meaningful functions.

An alternative point of view is that of assuming that librational dynamics does not contribute to thermal conductivity. The simplest function which satisfies the constraint of vanishing zero-time derivative and vanishing time integral, required to satisfy conservation laws, has a transform given by

$$\tilde{f}_D(z)=\frac{z^2+a_1z}{z^3+a_1z^2+b_1z+b_0}, \tag{3.3}$$

with a_1, b_1, and b_0 real and positive. In the time domain this becomes

$$f_D(t)=\frac{A_{12}}{B_{12}}\exp(-\gamma_{2D}t)\left(\cos(\omega_Dt)+\frac{2\gamma_{2D}C_{12}}{\omega_DA_{12}}\sin(\omega_Dt)\right)$$
$$-\frac{2\gamma_{1D}\gamma_{2D}}{C_{12}}\exp(-\gamma_{1D}t), \tag{3.4}$$

where

$$A_{12}=(\gamma_{1D}^2+\gamma_{2D}^2+\omega_D^2),$$
$$B_{12}=(\gamma_{1D}-\gamma_{2D})^2+\omega_D^2, \tag{3.5}$$
$$C_{12}=(\gamma_{2D}^2-\gamma_{1D}^2+\omega_D^2),$$

so that

$$a_1=\gamma_{1D}+2\gamma_{2D},$$
$$b_1=2\gamma_{1D}\gamma_{2D}+\gamma_{2D}^2+\omega_D^2, \tag{3.6}$$
$$b_0=\gamma_{1D}(\gamma_{2D}^2+\omega_D^2).$$

A fit with a combination of five functions of type (3.3), referred to as D, is also shown in Fig. 3. As γ_{1D} has been constrained to be equal to γ_{2D} the number of parameters for the D fit is 2 as for the L fit. As can be seen, the quality of the D fit for $\omega>80$ Thz is the same as that of the L fit, but the low-frequency part which we obtain subtracting the D function from the MD spectra is physically more meaningful.

The low-frequency part, in fact, can be well described by a combination of two exponentials and a ''cage mode.'' The faster exponential, which gives the ''normal'' contribution to λ, has a time rate of the same order as the inverse of the collision time (~ 0.03 ps for SPC/E, calculated as in [1]), while the slower exponential (the ''anomalous'' negative contribution) is only significant at 255 K. If the remaining cage mode is also described by a function such as Eq. (3.3), it turns out that the two exponentials yield the same contribution to thermal conductivity, irrespective of the formalism adopted, both at 255 and 300 K.

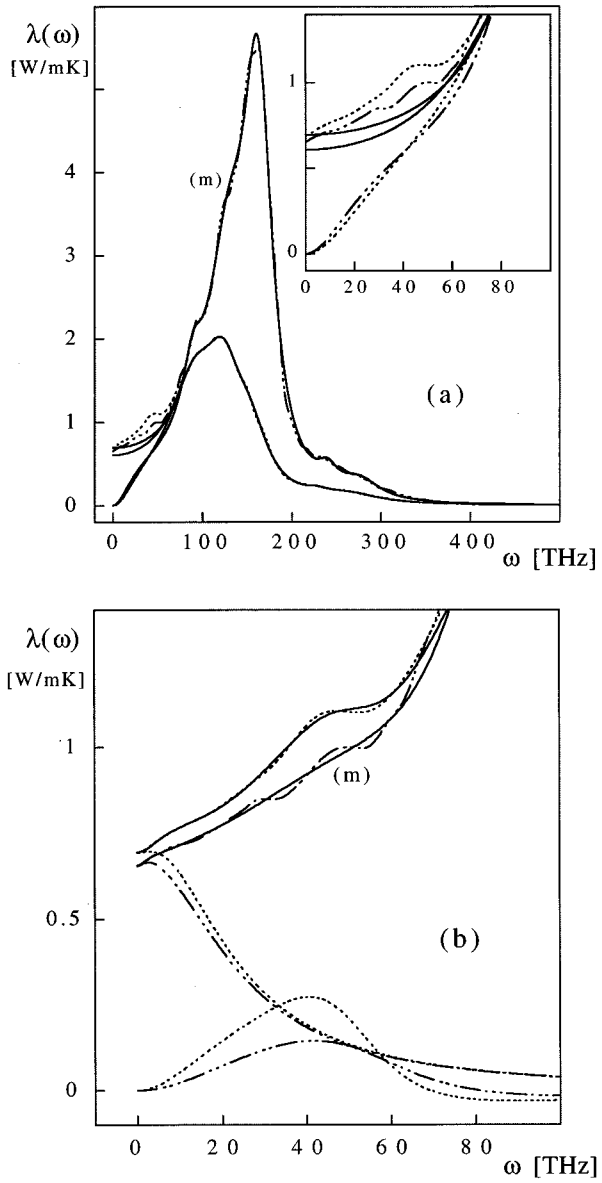

FIG. 4. Same as Fig. 3 at 300 K.

This is not obtained if the cage mode is described with an L function, hence we consider that the assumption of no contribution to thermal conductivity from high-frequency dynamics leads to a more satisfactory physical picture.

C. Generalized thermal conductivity and diffusivity

As already mentioned, $F_{55}(k,t)$ at finite k can be derived from $F_{33}(k,t)$ via conservation laws, Eq. (2.2). This, however, implies that the spectrum of $F_{55}(k,t)$ vanishes at $\omega=0$, exactly as in the case of $F_{44}(k,t)$ [2], the stress-tensor component correlation function, in view of its link with the longitudinal current CF, $F_{22}(k,t)$. As a consequence, the spectrum of $F_{55}(k,t)$ with its discontinuity between $k=0$ and all

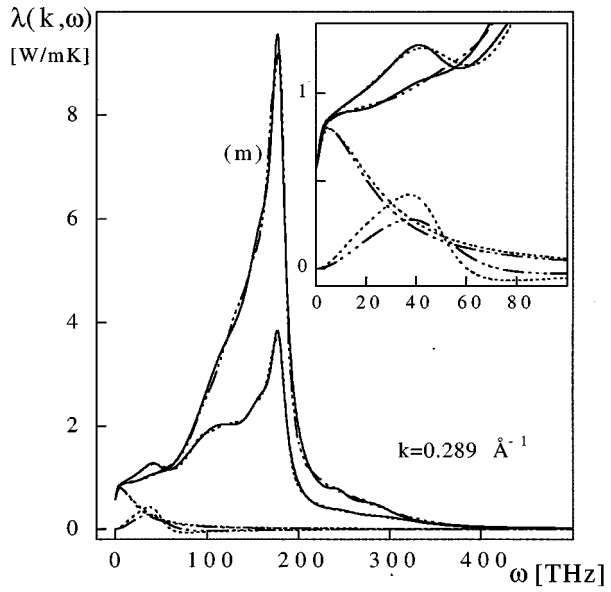

FIG. 5. $\lambda(k,\omega)$ at $k=k_{\min}$ and $T=255$ K [Eqs. (2.4), (2.5), and (2.9)]. The same functions as in Fig. 3(b) are shown and the inset details the low-frequency region.

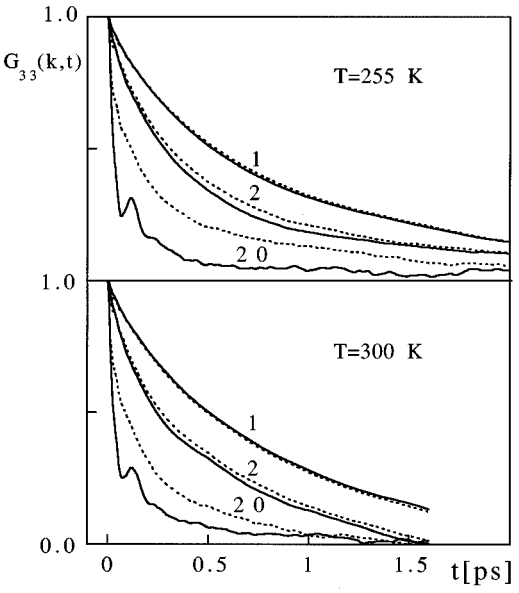

FIG. 6. Atomic (full curves) and molecular (dotted curves) $G_{33}(k,t)$ [Eq. (2.3)] at a few values of k. The curves are labeled according to the value of $(k/k_{\min})^2$.

finite k is of no help in computing generalized thermal conductivity. Rather, the latter can be obtained from $D_T(k,\omega)$, Eq. (2.9) through $G_{33}(k,t)$ and its spectrum, Eqs. (2.3)–(2.5), shown in Fig. 5. The values of $\lambda(k)$ we obtain this way at $k=k_{\min}$ are somewhat larger than at $k=0$, namely, $\lambda(k_{\min})=0.57$ W/mK vs 0.52 W/mK at 255 K and $\lambda(k_{\min})=0.69$ W/mK vs 0.67 W/mK at 300 K.

In the spectrum, Fig. 5, we observe an enhanced librational band, which is now sharply peaked at $\omega=170-175$ THz, i.e., at the frequency of the CF of the angular velocity component around an axis normal to the dipole axis, in the molecular plane [9]. At low frequencies, on the other hand, the contribution of the cage mode and, even more so, that of the two exponentials is essentially the same as at $k=0$. This supports the idea that transport parameters such as viscosity and thermal conductivity do not change significantly between $k=0$ and $k=k_{\min}$, unlike what is observed for, e.g., velocity and absorption of sound [1].

From the back transform of the spectrum shown in Fig. 5, $N_q(k,t)$ can be obtained and thus $n_q(k,t)$ and the characteristic frequency $f_{Tq}(k)$, Eq. (2.5). Its values at 255 K are $f_{Tq}(k_{\min})=28$ and 21 THz for the molecular and atomic function, respectively. The time integral of $n_q(k,t)$ is similar to that of $F_{55}(k,t)$ [Fig. 2(a)] with an analogous negative long-time tail. The time dependence of $n_q(k,t)$ is qualitatively very similar to that obtained for the TIP4P model at 245 K (see Figs. 17 and 18 of Ref. [1]), besides the librational oscillations, that were subtracted in [1] from $F_{33}(k,t)$ [and hence $G_{33}(k,t)$] at the outset for the TIP4P model. Again, the main difference between the SPC/E and TIP4P results for $n_q(k,t)$ is in the decay rate of the long-time tails [see Eqs. (3.8) and (3.9)], which is slower for the SPC/E water model, $\gamma_1^{(N)}\approx 2-3$ THz at 255 K vs $\gamma_1^{(N)}\approx 4-9$ THz at 245 K for TIP4P, see Table X in [1].

Generalized thermal diffusivity $D_T(k)$ can also be obtained more straightforwardly from the time dependence of $G_{33}(k,t)$, Fig. 6, which in the hydrodynamic limit becomes exponential, $G_{33}(k,t)\simeq\exp[-D_T(k)k^2t]$. As can be seen, this limit is almost reached for the two smallest k's where ''atomic'' and ''molecular'' functions almost coincide. The two functions, on the other hand, differ remarkably at $k^2=20$, where they decay faster, with an oscillation of the frequency of the cage mode, much more visible in the atomic results.

The values of $D_T(k)$, obtained extrapolating the integral of $G_{33}(k,t)$ to $t\to\infty$, are shown in Fig. 7. In addition to atomic and molecular values, the curve (hyd) presents results obtained from the following decomposition of the integral of $G_{33}(k,t)$ into a fast and a slow part, assumed to decay exponentially:

$$\int_0^\tau G_{33}(k,t)dt = I_{\mathrm{HF}}(k,\tau)+I_{(\mathrm{hyd})}(k)(1-e^{-D_T^{(\mathrm{hyd})}(k)k^2\tau}). \tag{3.7}$$

Overall, $D_T(k)$ decreases as a function of k, irrespective of the method used to calculate it and at both temperatures.

On the other hand, while $D_T^{(\mathrm{hyd})}(k)$ is the same for atomic and molecular data, the molecular results decay faster than the atomic ones at both temperatures, after being equal at $k=k_{\min}$. It should also be noted that $D_T(k)$ is smaller at $k=0$ than at $k=k_{\min}$. This apparently anomalous feature and the faster decay of the molecular values can be accounted for if the contribution to $G_{33}(k,t)$ of the various dynamic modes is taken into account as follows.

$G_{33}(k,t)$ is fitted with a combination of four complex exponentials. Two of them represent the librational and cage mode contributions, with amplitude $A_{\mathrm{lib}}(k)$ and $A_{\mathrm{cage}}(k)$, respectively. The remaining two exponentials [with amplitude $A_{\mathrm{hyd}}(k)$ and $A_{\mathrm{coll}}(k)$] describe the low frequency related to the hydrodynamic contributions to $N_q(k,t)$. As already mentioned (see Figs. 2–5), the low-frequency part of $N_q(k,t)$ is

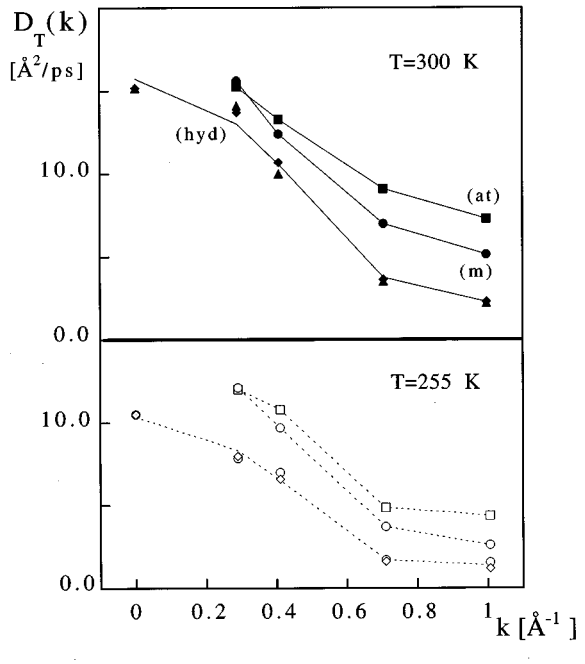

FIG. 7. Generalized thermal diffusivity as a function of k [Eq. (2.4)]. Atomic (squares) and molecular (circles) results are shown. The curves labeled (hyd) display $D_T(k)$ obtained from Eq. (3.7). The latter are the same for atomic and molecular (m) data, within the error.

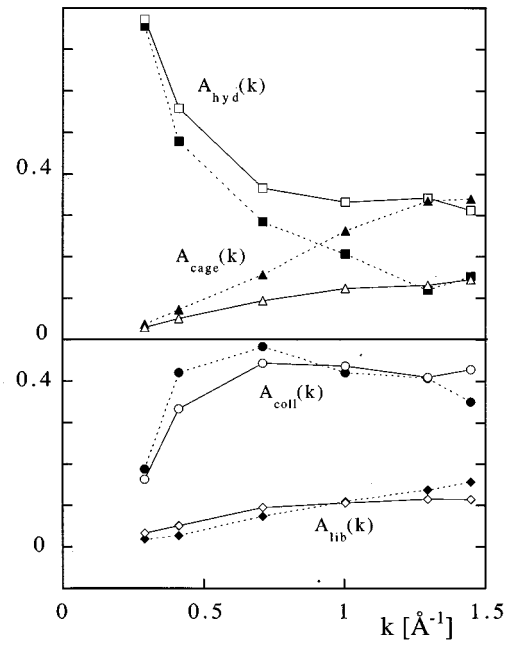

FIG. 8. Contribution of the dynamic modes to $G_{33}(k,t)$. Molecular (open symbols) and atomic (filled symbols) results obtained fitting $G_{33}(k,t)$ with four complex exponentials, see text. $T=255$ K.

composed of a ''normal'' mode, with positive amplitude and an ''anomalous'' mode with negative amplitude. The amplitudes of these four modes are shown in Fig. 8 as a function of k. As can be seen, the main contribution to the integral comes from the ''hydrodynamic'' and from the ''collective'' modes, which both are functions of the ''normal'' and ''anomalous'' modes of $N_q(k,t)$.

Alternatively, an approximate description of the modes of $G_{33}(k,t)$ can be obtained from the spectrum of $N_q(k,t)$, through Eq. (2.5). We restrict this description to the low-frequency region, both for its importance for $\lambda(k)$ and for numerical convenience.

From this equation we obtain

$$\tilde{G}_{33}^{(\mathrm{hyd})}(k,z)\approx\frac{1}{z+f_{Tq}^{(BF)^2}\left(\dfrac{(1+\alpha_1)}{z+\gamma_c^{(N)}}-\dfrac{\alpha_1}{z+\gamma_1^{(N)}}\right)}=\frac{z^2+[2\gamma_c^{(G)}+\gamma_1^{(G)}]z+\alpha_1^{(G)}\{\omega_c^{(G)^2}+[\gamma_c^{(G)}-\gamma_1^{(G)}]^2\}+2\gamma_c^{(G)}\gamma_1^{(G)}}{z^3+[2\gamma_c^{(G)}+\gamma_1^{(G)}]z^2+[2\gamma_c^{(G)}\gamma_1^{(G)}+\omega_c^{(G)^2}+\gamma_c^{(G)^2}]z+\gamma_1^{(G)}[\omega_c^{(G)^2}+\gamma_c^{(G)^2}]},\tag{3.8}$$

where the superscripts (N) and (G) relate to $N_q(k,t)$ and $G_{33}(k,t)$, the subscripts c and l stand for collisional and long-time mode, and the k dependence of the coefficients is omitted.

The rightmost term of Eq. (3.8) is the linear combination of an exponential and a complex exponential of the type L, Eq. (3.1), with the constraint of vanishing time derivative at $t=0$.

Equating terms of the same order in z, we obtain the following system of equations:

$$\gamma_1^{(G)^3}-[\gamma_c^{(N)}+\gamma_1^{(N)}]\gamma_1^{(G)^2}+[f_{Tq}^{(BF)^2}+\gamma_c^{(N)}\gamma_1^{(N)}]\gamma_1^{(G)}-f_{Tq}^{(BF)^2}[(1+\alpha_1)\gamma_1^{(N)}-\alpha_1\gamma_c^{(N)}]=0,$$

$$\gamma_c^{(G)}=\frac{[\gamma_c^{(N)}+\gamma_1^{(N)}-\gamma_1^{(G)}]}{2},$$

$$\omega_c^{(G)^2}=\frac{f_{Tq}^{(BF)^2}}{\gamma_1^{(G)}}[(1+\alpha_1)\gamma_1^{(N)}-\alpha_1\gamma_c^{(N)}]-\gamma_c^{(G)^2},$$

$$\alpha_1^{(G)}=\frac{\gamma_c^{(N)}\gamma_1^{(N)}-2\gamma_c^{(G)}\gamma_1^{(G)}}{\omega_c^{(G)^2}+(\gamma_c^{(G)}-\gamma_1^{(G)})^2}.\tag{3.9}$$

Solving Eq. (3.9), the low-frequency parameters of $G_{33}(k,t)$ can be obtained from that of $N_q(k,t)$, $\gamma_1^{(N)}\approx 2-3$ THz and $\gamma_c^{(N)}\approx 20-30$ THz at 255 K, for $k<0.8$ Å^{-1}. The results are in good agreement with that directly obtained from the fit of $G_{33}(k,t)$, in that $G_{33}(k,t)$ turns out to be composed, in the

TABLE II. (a) Calculated molecular (m) and atomic (at) initial values of $F_{11}(k,t)$, $F_{13}(k,t)$, and $F_{33}(k,t)$. (b) Calculated molecular (m) and atomic (at) initial values of $F_{22}(k,t)$, $F_{25}(k,t)$, $F_{44}(k,t)$, and $F_{55}(k,t)$.

(a)

k (Å^{-1})	V_{11}(at.)	$V_{11}(m)$	$V_{13}(at)$ (kJ/mol)	$V_{13}(m)$ (kJ/mol)	$V_{33}(at)$ (kJ/mol)^2	$V_{33}(m)$ (kJ/mol)^2
			$T=300$ K			
0.00						
0.2876	0.065	0.065	−2.754	−2.821	179.5	185.4
0.4068	0.068	0.069	−2.984	−3.036	192.6	198.8
0.7046	0.086	0.086	−3.596	−3.641	221.4	222.5
0.9965	0.119	0.122	−4.899	−4.946	286.2	271.8
1.2864	0.232	0.239	−9.346	−9.288	493.2	438.5
1.4383	0.309	0.322	−12.69	−12.71	650.3	577.2
2.0743	0.946	1.040	−35.78	−37.99	1594	1464
2.8766	1.120	1.435	−39.37	−55.05	1746	2186
4.3149	0.692	0.879	−25.62	−33.21	1429	1332
5.7532	0.774	1.008	−27.87	−38.04	1453	1510
8.6298	0.773	0.965	−28.77	−36.37	1443	1448
14.383	0.808	1.003	−29.68	−38.08	1467	1522
28.766	0.791	0.998	−29.37	−37.72	1502	1502
40.272	0.800	1.000	−29.76	−37.78	1510	1503
			$T=255$ K			
0.00						
0.2895	0.050	0.050	−2.095	−2.157	136.2	142.7
0.4095	0.045	0.046	−1.911	−1.954	131.1	136.1
0.7092	0.064	0.064	−2.702	−2.746	173.8	175.4
1.0030	0.104	0.106	−4.567	−4.656	271.3	265.3
1.2949	0.209	0.215	−8.946	−9.168	472.0	453.3
1.4477	0.308	0.317	−13.42	−13.86	688.0	666.2
2.0880	0.946	1.030	−38.96	−42.25	1795	1789
2.8955	1.150	1.470	−42.70	−62.70	1896	2725
4.3432	0.660	0.841	−26.09	−35.06	1417	1523
5.7910	0.659	0.843	−25.40	−35.21	1340	1531
8.6865	0.753	0.924	−29.51	−38.52	1475	1663
14.477	0.834	1.030	−32.71	−43.20	1595	1874
28.955	0.788	0.995	−30.59	−41.63	1528	1800
40.537	0.791	0.996	−31.12	−41.79	1553	1812

(b)

k (Å^{-1})	$V_{22}(at)$ [(Å/ps)^2]	$V_{22}(m)$ [(Å/ps)^2]	$V_{55}(at)$ [10^5 (Å kJ/mol ps)^2]	$V_{55}(m)$ [10^5 (Å kJ/mol ps)^2]	$V_{44}(at)$ [10^4 (Å/ps)^4]	$V_{44}(m)$ [10^4 (Å/ps)^4]	$V_{25}(at)$ (Å^2 kJ/ps^2 mol)	$V_{25}(m)$ (Å^2 kJ/ps^2 mol)
				$T=300$ K				
0.00			2.338	4.747				
0.2876	13.63	13.60	2.900	4.936	3.504	3.530	−526.8	−496.1
0.4068	13.35	13.35	2.802	4.337			−536.3	−509.4
0.7046	14.01	14.19	2.808	3.122	3.158	3.026	−671.0	−438.8
0.9965	13.85	14.21	2.869	2.212	2.477	2.546	−782.8	−426.1
1.2864	13.19	13.74	2.934	1.598	1.806	1.823	−857.0	−440.2
1.4383	13.46	14.15	2.889	1.338	1.469	1.515	−894.3	−472.6
2.0743	12.69	13.95	2.692	0.714	0.629	0.572	−808.2	−508.6
2.8766	12.29	14.05	2.393	0.422	0.353	0.218	−523.0	−493.3
4.3149	11.34	13.34	1.456	0.298	0.257	0.165	−376.1	−475.5
5.7532	12.23	13.97	0.950	0.251	0.186	0.111	−358.9	−494.8
8.6298	13.01	14.52	0.655	0.226	0.135	0.088	−444.9	−522.9
14.383	12.22	13.54	0.480	0.192	0.101	0.065	−402.7	−479.6
28.766	12.44	13.87	0.33	0.186	0.085	0.059	−441.6	−491.9
40.272	12.41	13.96	0.26	0.183	0.085	0.058	−447.2	−494.8

TABLE II. *(Continued).*

				$T=255$ K				
0.00			1.827	3.848				
0.2895	12.20	12.22	2.310	4.332	3.230	3.256	−529.3	−497.4
0.4095	11.73	11.78	2.242	3.749	3.131	3.160	−523.6	−449.7
0.7092	11.65	11.81	2.268	2.597	2.712	2.741	−626.0	−412.4
1.0030	11.29	11.59	2.352	1.819	2.149	2.213	−713.3	−387.9
1.2949	11.23	11.71	2.385	1.311	1.608	1.632	−800.7	−425.3
1.4477	11.19	11.78	2.360	1.111	1.339	1.356	−821.3	−447.1
2.0880	10.74	11.77	2.274	0.621	0.525	0.481	−756.4	−481.2
2.8955	10.34	11.89	2.009	0.392	0.290	0.193	−494.6	−472.6
4.3432	9.98	11.94	1.177	0.293	0.220	0.147	−380.0	−474.7
5.7910	10.31	11.73	0.766	0.244	0.154	0.094	−335.1	−463.9
8.6865	11.13	12.10	0.518	0.222	0.105	0.066	−419.0	−481.5
14.477	10.73	11.70	0.390	0.201	0.074	0.049	−392.7	−463.7
28.955	10.54	12.04	0.24	0.20	0.061	0.043	−404.9	−480.4
40.537	10.56	11.89	0.19	0.19	0.061	0.042	−418.0	−477.8

long-time regime, of two modes with positive amplitude, as opposed to that of $N_q(k,t)$. The first is a slow exponential with a rate $\gamma_1^{(G)} \approx 0.7$ to 0.8 THz at 255 K and a damped L-type mode with $\gamma_c^{(G)} > \omega_c^{(G)}$ ($\gamma_c^{(G)} \approx 10-15$ THz at 255 K), for $k < 0.8$ Å^{-1}.

At the lowest k, the atomic and molecular results are the same for the two modes, but the collision mode has a larger contribution to $D_T(k)$ than the hydrodynamic mode. The amplitude of the collision mode, as that of the other nonhydrodynamic modes, goes to zero when k goes to zero, compensating the increase of the amplitude of the hydrodynamic mode, Fig. 8. This effect is more apparent at 255 K, where the difference of contribution to $D_T(k)$ of the two modes is larger.

Also, the growing difference between atomic and molecular $D_T(k)$ (Fig. 7) is due to the larger amplitude of the hydrodynamic mode of the molecular $G_{33}(k,t)$ with a consequent smaller contribution to $D_T(k)$ and $\lambda(k)$. Notice the correlation between the amplitude of the hydrodynamic mode of Fig. 8 and the difference between atomic and molecular thermal diffusivity of Fig. 7.

D. Generalized thermodynamic properties

Tables II(a) and II(b) collect the initial values $V_{ij}(k)$ of the computed CF's $F_{ij}(k,t)$ at both temperatures. To analyze these data it is convenient to define a function $\Gamma_{ij}(k)$ as follows:

$$\Gamma_{ij}^{(C,at)}(k) = \frac{V_{ij}^{(at)}(k) - V_{ij}^{(S,at)}(k)}{V_{ij}^{(S,m)}(k \to \infty)}, \tag{3.10}$$

$$\Gamma_{ij}^{(C,m)}(k) = \frac{V_{ij}^{(m)}(k) - V_{ij}^{(S,m)}(k)}{V_{ij}^{(S,m)}(k \to \infty)}. \tag{3.11}$$

These functions extract the collective, or cross (C), part of the relevant CF and normalize it to the $k \to \infty$ limit of the single-molecule, or self (S), contribution of the molecular function. For instance, we obtain for the density-density CF

$$\Gamma_{11}^{(C,at)}(k) = V_{11}^{(at)}(k) - V_{11}^{(S,at)}(k), \tag{3.12}$$

$$\Gamma_{11}^{(C,m)}(k) = V_{11}^{(m)}(k) - 1 \equiv S^{(m)}(k) - 1. \tag{3.13}$$

The latter function is the cross part of the amplitude of the intermediate scattering function correspondent to the center of mass of the water molecules, $F_{11}(k,t)$.

The k dependences of $\Gamma_{ij}^{(C)}(k)$ for the three independent CF's $F_{11}(k,t)$, $F_{13}(k,t)$, and $F_{33}(k,t)$ are shown in Fig. 9. As can be seen, the molecular results coincide at all k's, while the atomic values are somewhat dispersed, mainly around the maximum of the curve.

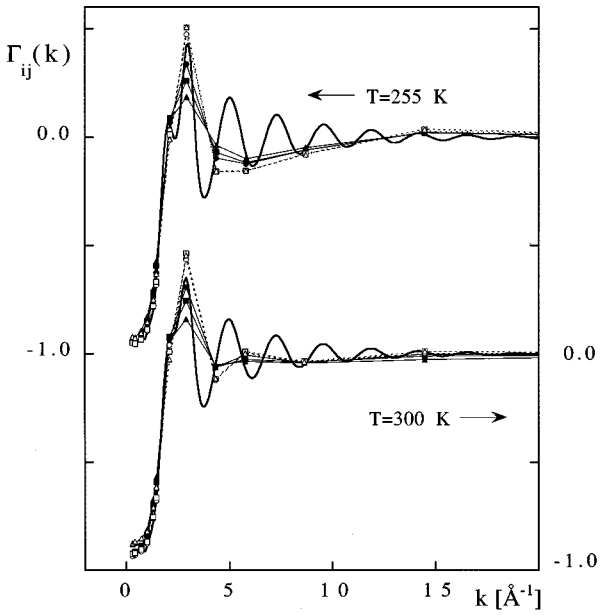

FIG. 9. Normalized collective part of $V_{11}(k)$ (circles), $V_{13}(k)$ (squares), and $V_{33}(k)$ (triangles), Eqs. (3.10), (3.11). Molecular (open symbols) and atomic (filled symbols) results. The full heavy curves show the O-O partial structure functions.

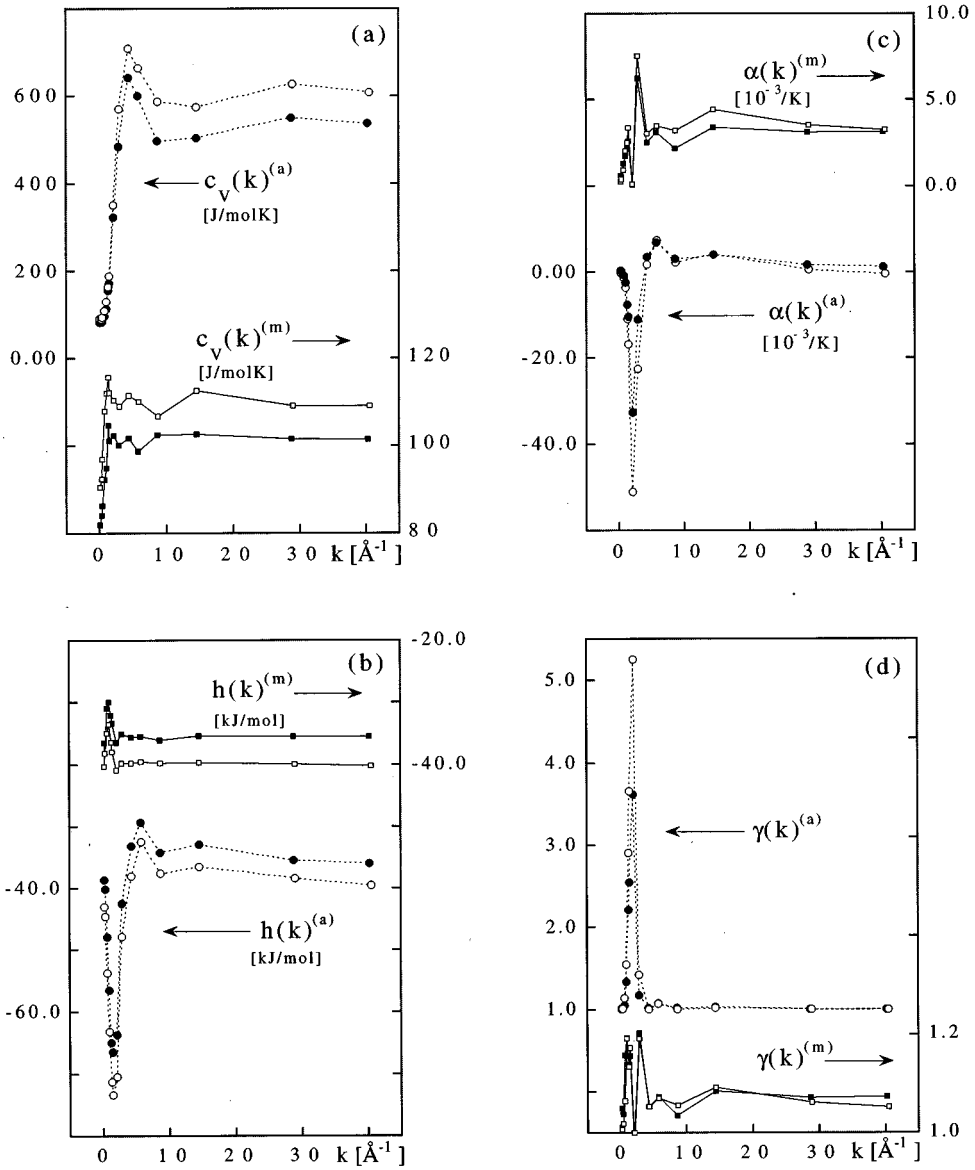

FIG. 10. Generalized thermodynamic functions. Molecular and atomic results at 300 K (filled symbols) and 255 K (open symbols).

This shows that the behavior of the three molecular CF's is determined by the (Fourier transform of) the radial distribution function of the center of mass, $g(r)$, i.e.,

$$\Gamma_{ij}^{(C,m)}(k)=4\pi\rho\int_0^\infty r^2[g(r)-1]\,\frac{\sin(kr)}{kr}\,dr. \quad (3.14)$$

The analogous relation for the atomic part can be obtained generalizing Eq. (3.14) to water [25]:

$$\Gamma_{ij}^{(C,at)}(k)=\frac{4m_{\mathrm{H}}^2}{M^2}\,S_{\mathrm{HH}}(k)+\frac{4m_{\mathrm{H}}m_{\mathrm{O}}}{M^2}\,S_{\mathrm{OH}}(k)+\frac{m_{\mathrm{O}}^2}{M^2}\,S_{\mathrm{OO}}(k), \quad (3.15)$$

where

$$S_{ij}(k)=4\pi\rho\int_0^\infty r^2[g_{ij}(r)-1]\,\frac{\sin(kr)}{kr}\,dr. \quad (3.16)$$

Hence we can attribute the smaller peak of the atomic functions to the contribution of the O-H pair, which is minimum at $k=2.9$ Å^{-1}, where the O-O correlation has its maximum.

From the data given in Table II the generalized thermodynamic properties heat capacity, $c_P(k)$ and $c_V(k)$, thermal expansivity $\alpha(k)$, and enthalpy per molecule, $h(k)$, can be calculated by means of Eqs. (2.11)–(2.14). The results are shown in Fig. 10.

As for $c_V(k)$, the most apparent feature visible in Fig. 10(a) is the large increase of the atomic data, roughly five to six times larger than the corresponding molecular values at the largest k's. The moderate ($\sim$20%) increase of the latter is to be attributed to the cross term while the self part, essentially k independent, is $c_V^{(S,m)}(k\to\infty)\approx 100$ and ≈ 110 J/mol K at 300 and 255 K, respectively. The values obtained at $k=0$ from Eq. (2.9) are $c_V(k=0)\approx 82$ J/mol K at 300 K and $c_V(k=0)\approx 90.5$ J/mol K at 255 K, in good agreement with the results at $k=k_{\min}$.

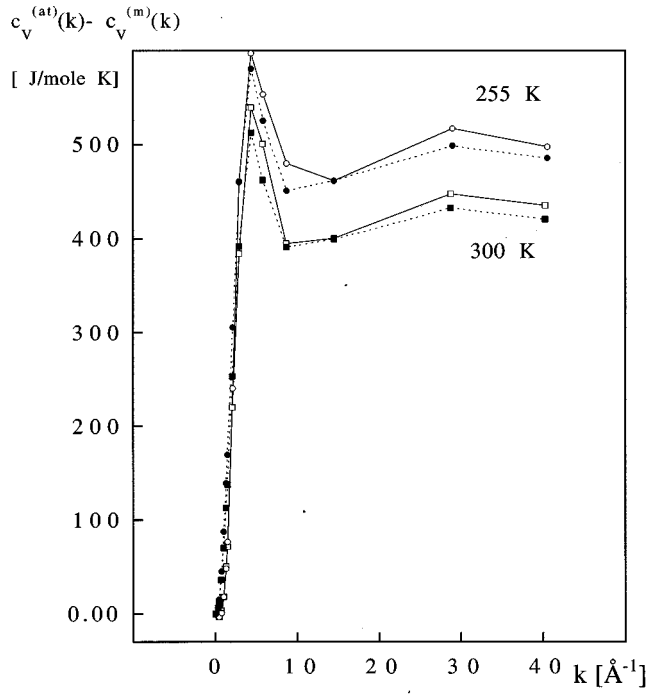

FIG. 11. Difference between atomic and molecular results of constant volume specific heat. MD (open symbols) and computed [Eq. (3.17)] results.

On the contrary, the difference between atomic and molecular $c_V(k)$ is due to the self part of the $V_{ij}(k)$ used to calculate specific heat through Eq. (2.12). Actually, exploiting the analogy of behavior apparent in Fig. 9 we obtain

$$k_B T^2[c_V^{(at)}(k) - c_V^{(m)}(k)] \cong V_{33}^{(S,at)}(k) - V_{33}^{(S,m)} + [V_{13}^{(S,m)}(\infty)]^2 \times [1 - V_{11}^{(S,at)}(k) - 2\delta_{13}(k)], \tag{3.17}$$

where

$$\delta_{13}(k) = \frac{V_{13}^{(S,at)}(k)}{V_{13}^{(S,m)}(\infty)} - V_{11}^{(S,at)}(k). \tag{3.18}$$

To obtain Eq. (3.17), we also assumed the cross terms equal for atomic and molecular functions (see Fig. 9) and $\delta_{13}(k) \ll 1$. In fact, from Eqs. (2.15) and (2.16) we have $\delta_{13}(k \to \infty) \approx 0.01$ at 300 K and $\delta_{13}(k \to \infty) \approx 0.05$ at 255 K. Notice that the right-hand side of Eq. (3.17) is only composed of self (rotational) terms containing spherical Bessel functions, Eqs. (2.15)–(2.21).

The difference between atomic and molecular $c_V(k)$ is shown in Fig. 11 as a function of k and compared to that obtained from Eq. (3.17). The good agreement between the two curves proves that this large difference is almost totally due to single-molecule effects. From an analysis of the contribution of the various modes, as was done for the curves of Fig. 8, we find that most of the observed difference is due to the cage mode, i.e., the dynamics whose frequency components are centered at ~ 45 THz, whose amplitude is twice as large for the atomic function as that of the molecular one.

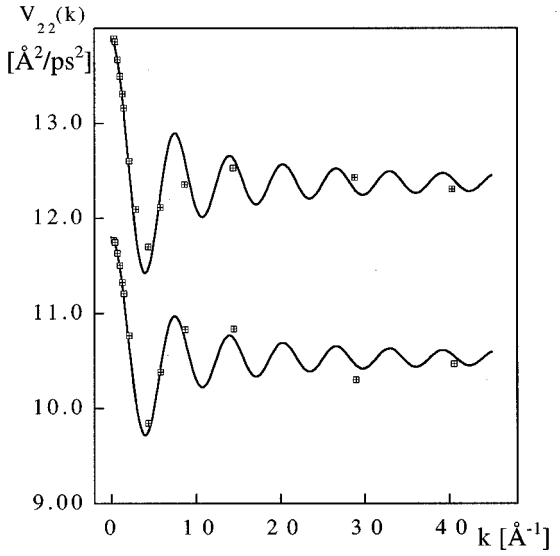

FIG. 12. Comparison of MD (symbols) and theoretical [full curves, Eq. (2.19)] results of the initial value of the longitudinal current.

A striking difference between molecular and atomic results is exhibited by the k dependence of $h(k) = V_{25}(k)/V_{22}(k)$, the generalized enthalpy per molecule, Fig. 10(b). The first has a maximum at ~ 1 Å^{-1}, about 25–30 % larger than at $k=0$, while the latter shows a deep minimum at ~ 1.6 Å^{-1}, where the amplitude almost doubles. In this case, the single-molecule molecular term does not depend on k, and the k dependence of the corresponding atomic data cannot account for the behavior observed in Fig. 10(b). This is mainly determined by the numerator, $V_{25}(k)$. In fact, $V_{22}^{(m)}$ does not depend on k, while the k dependence of $V_{22}^{(\text{at.})}(k)$, shown in Fig. 12, is clearly very different from that of $h(k)$. Hence we conclude that the behavior of $h(k)$ is due to collective effects.

The contribution of the various modes can be estimated from the spectra of $F_{25}(k,t)$, shown in Fig. 13(a) at a few k values. These spectra have been normalized to $V_{25}^{(S,m)}(\infty)$ to allow a more homogeneous comparison. A hydrodynamic mode, whose peak shifts in frequency with k, a bending mode (8–10 THz), and a cage mode can be detected in these spectra. The latter mode has the largest difference of amplitude between atomic and molecular results.

The comparison of Fig. 13(b) between the spectra of $F_{25}(k,t)$ and $F_{22}(k,t)$, normalized as above, further shows that, at $k=1$ Å^{-1}, where the maximum of $h^{(m)}(k)$ is, the amplitude of the cage mode of $F_{25}(k,t)$ is larger than that of $F_{22}(k,t)$ for the atomic function, but smaller for the molecular one.

Strong evidence supporting the above hypothesis of a dominant role played by collective interactions in determining the behavior of $h(k)$ is provided by the results shown in Fig. 14(a). In the atomic case, the function $V_{25}(k)$ has been decomposed into a kinetic and a potential part, according to Eq. (2.22) [$F_{25}(k,t) = F_{34}(k,t)$]. At low k, the potential term is much larger than the kinetic, while the opposite is true at intermediate to large k, where the potential term decays to zero. The combination of the two terms leads to a

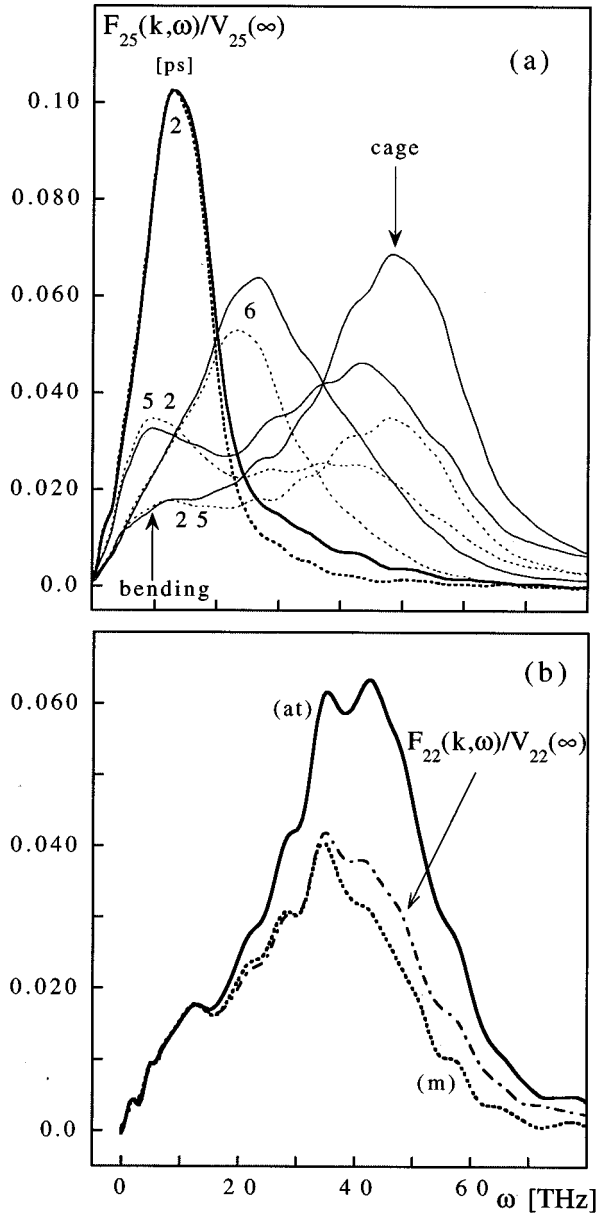

FIG. 13. (a) Spectra of atomic (full curve) and molecular (dotted curve) $F_{25}(k,t)$, normalized to the high-k limit of molecular V_{25}. The number on the curves indicates $(k/k_{\min})^2$ and the arrows a typical peak position of the O-O-O bending mode and cage mode, $T=255$ K. (b) Comparison of the spectra of $F_{25}(k,t)$ and $F_{22}(k,t)$, normalized as above, at $k=1$ Å^{-1}, the k value of the maximum of the molecular $h(k)$, see Fig. 10(b).

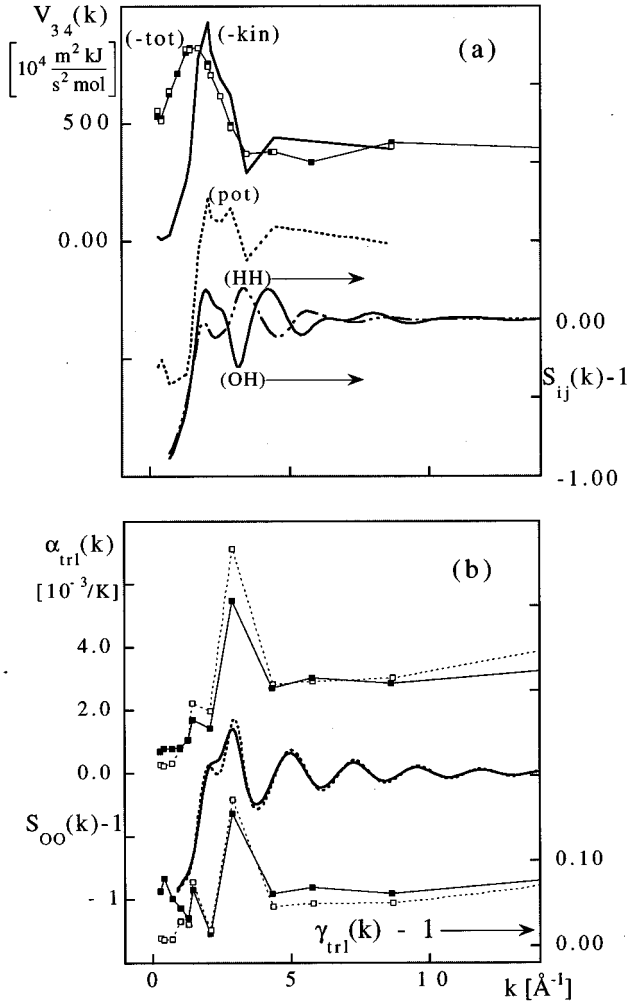

FIG. 14. (a) k dependence of the kinetic (kin) and potential (pot) contributions to $V_{25}(k)$ calculated in the atomic formalism at 255 K. The scale on the right relates to the partial structure functions for the O-H and H-H pairs. (b) k dependence of the translational part of $\alpha(k)$ and $\gamma(k)-1$ (see text) at 300 K (filled symbols) and 255 K (open symbols). The lines are an aid to the eye. For the sake of comparison, also the O-O structure functions at the corresponding temperatures are shown.

shift of the peak maximum to lower k's (~ 1.6 Å^{-1}) compared to that of the separate components, which both peak at ~ 2 Å^{-1}. There is an apparent correlation between the position of the maximum of $V_{25}^{(\mathrm{pot})}(k)$ and $V_{25}^{(\mathrm{kin})}(k)$ and that of the first maxima of the partial structure functions [Eq. (3.16)]. Presumably, a similar shift also occurs in the molecular case, likely to a larger extent.

If we introduce a ''translational'' generalized enthalpy

$$h_{\infty}^{\mathrm{trl}}=\frac{V_{25}^{(S,m)}(\infty)}{V_{22}^{(S,m)}(\infty)}=\frac{V_{25}^{(S,at)}(\infty)}{V_{22}^{(S,at)}(\infty)}, \tag{3.19}$$

whose value is the same for atomic and molecular formalism, we can conclude that, at intermediate k's, intermolecular rotational effects produce a larger or smaller amplitude of the cage mode, that leads to a minimum of $h^{(at)}(k)$, or a maximum of $h^{(m)}(k)$, located on opposite sides with respect to the translational value $h_{\infty}^{\mathrm{trl}}$ of Eq. (3.19).

On the other hand, either in the $k\rightarrow 0$ limit, where the hydrodynamic mode dominates, or in the $k\rightarrow\infty$ limit (free-particle behavior) both definitions lead to the same value $h_{\infty}^{\mathrm{trl}}$.

In view of Eqs. (2.10) and (2.12) also the constant pressure heat capacity $c_p(k)$ and hence the ratio $\gamma(k)$, as well as the thermal expansion coefficient $\alpha(k)$ will have a k dependence that is determined by that of $h(k)$ and $c_v(k)$. Actually, we can write for $\alpha(k)$

$$k_B T^2 \alpha^{(m,at)}(k)\cong k_B T^2 \alpha_{\mathrm{trl}}^{(m,at)}(k)+k_B T^2 \alpha_{\mathrm{rot}}^{(m,at)}(k), \tag{3.20}$$

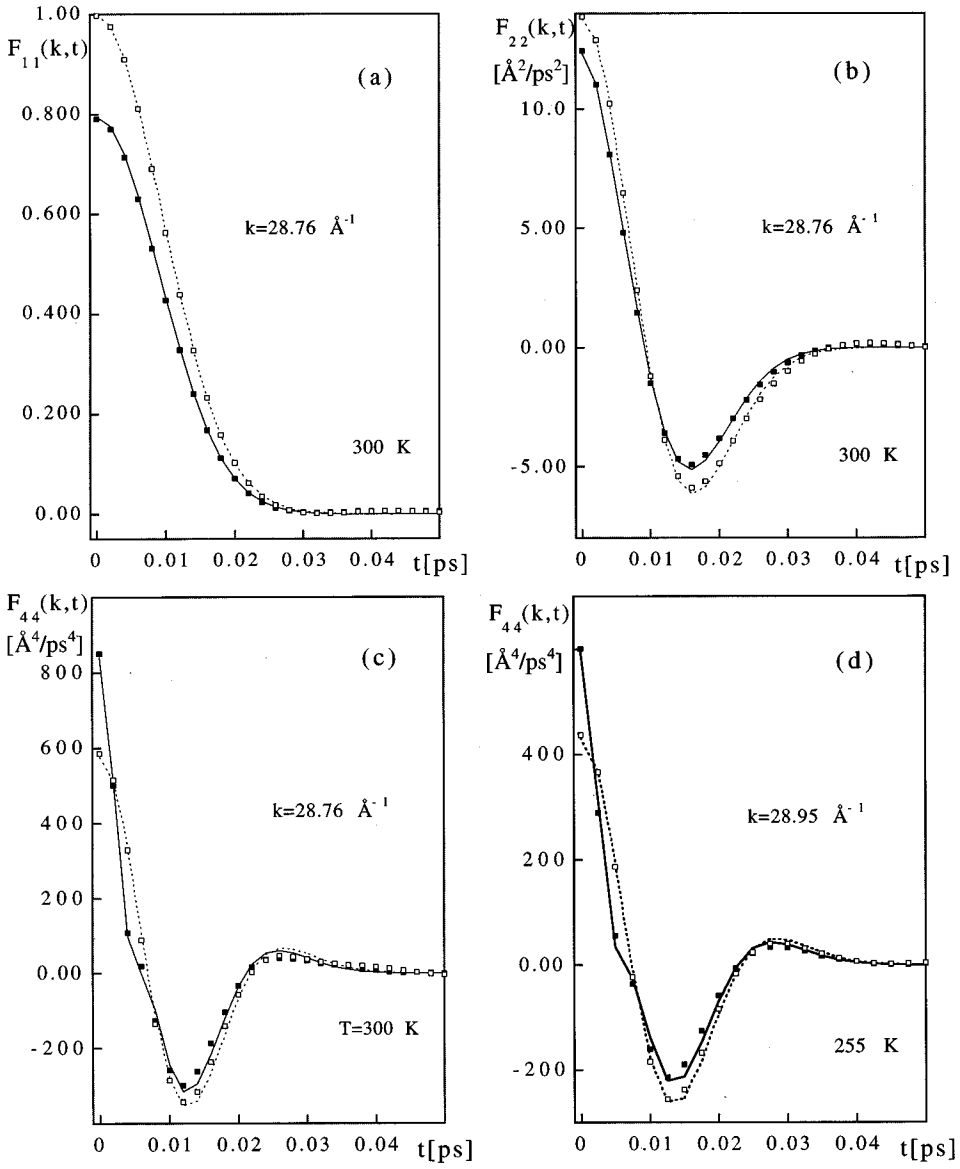

FIG. 15. Very-high-k behavior of some $F_{ij}(k,t)$. Comparison of MD results (symbols) with those obtained from Eq. (2.22) and conservation laws at $k=100k_{\min}$. Molecular results: open symbols; atomic results: filled symbols.

where

$$k_B T^2 \alpha_{\rm trl}^{(m)}(k)=[1+V_{11}^{(C)}(k)]\left(h_\infty^{\rm trl}-\frac{V_{13}^{(m)}(\infty)}{V_{11}^{(m)}(\infty)}\right), \tag{3.21}$$

$$k_B T^2 \alpha_{\rm rot}^{(m)}(k)=[1+V_{11}^{(C)}(k)][h^{(m)}(k)-h_\infty^{\rm trl}], \tag{3.22}$$

and

$$\alpha_{\rm tr}^{(at)}(k)=\alpha_{\rm trl}^{(m)}(k),$$

$$k_B T^2 \alpha_{\rm rot}^{(at)}(k)=(V_{11}^{(S,at)}-1)\left(h_\infty^{\rm trl}-\frac{V_{13}^{(m)}(\infty)}{V_{11}^{(m)}(\infty)}\right)+[1+V_{11}^{(C)}(k)]$$
$$\times[h^{(m)}(k)-h_\infty^{\rm trl}]. \tag{3.23}$$

The convenience of Eq. (3.23) is that it extracts the dependence of $\alpha(k)$ on rotational motions.

Equation (2.12) that gives $\gamma(k)-1$, the ratio of specific heats, depends at the numerator on $[\alpha(k)]^2$ and, at the denominator, on $c_v(k)$, so that the sharp peak of the atomic results, Fig. 10(d), is to be related to that of $\alpha(k)$. On the other hand, the two peaks of the molecular results are due to the combined effect of $\alpha(k)$ and $c_v(k)$, as can be seen from Figs. 10(a) and 10(c).

The difference observed in the k dependence of the molecular and atomic values of $c_v(k)$, $h(k)$, $\alpha(k)$, and $\gamma(k)$ has been traced back to rotational terms typically in the frequency range around 45 THz. This point of view is supported by the results obtained for the translational part of the above functions, computed from Eq. (3.19), setting $h=h_\infty^{\rm trl}$ and assuming the molecular data for the translational $c_v(k)$, see Fig. 14(b) for $\alpha(k)$ and $\gamma(k)$. As can be seen, the shape

of both these functions closely resembles that of $S(k)$ at the relevant temperatures.

$\alpha(0)$, obtained extrapolating to $k=0$ the data of Table II, is in agreement with that given by Eq. (3.21), Fig. 14(b), and positive at both temperatures, namely, $+[2\pm1]\times10^{-4}$/K at 255 K and $+[5.5\pm1.5]\times10^{-4}$/K at 300 K, to be compared with the corresponding experimental values -5.8×10^{-4}/K [13] and $+2.8\times10^{-4}$/K [14]. The disagreement at 255 K is an evidence that the density maximum of the SPC/E water model is shifted to lower temperatures than that of real water, as also observed for the TIP4P model [26].

Note that at all k's considered $\gamma^{(m)}(k)<1.2$. This confirms the lack of significant coupling between fluctuations of density and energy in water. A further proof of this is provided by the small values of $G_{13}(k,t)$ at all k's, that indicate negligible coupling between stress tensor and heat flux fluctuations [1,5].

E. Free-streaming limits

At large k, say $k>10$ Å^{-1}, the time dependence of the computed CF's changes from a linear combination of complex exponentials into a Gaussian one. In this limit, the spectral bands relevant to the various modes broaden and merge with each other, so that the spectrum becomes similar to that of a free motion.

The difference between an atomic and a molecular liquid, of course, is that the rotational motion of the molecular liquid requires a second Gaussian to describe the CF. Actually, the coefficients A_{RH} and A_{RO} in the argument of the two Gaussians [atomic definition, Eqs. (2.23)–(2.26)] both contain a translational term for the center of mass and molecular rotational terms. The molecular definitions, conversely, are quite analogous to that for a hard-sphere fluid [10], except that the interaction potential makes $V_{13}(k)\neq0$ here.

The agreement between Eqs. (2.23)–(2.26) and the MD results is very good and the MD coefficients agree with that obtained from the fit of the atomic CF's, despite the small contribution of the hydrogen compared to that of the oxygen. As an example, we show in Fig. 15 the MD results of $F_{11}(k,t)$, $F_{22}(k,t)$, and $F_{44}(k,t)$ together with that computed according to Eqs. (2.23) and conservation laws, for $k=100k_{\min}$.

The Gaussian relevant to the hydrogen dynamics can only be seen in $F_{44}^{(at)}(k,t)$, being much too small in the other two CF's. This Gaussian is about three times narrower than that of the oxygen, which is very similar to that of the center of mass. However, $F_{44}^{(at)}(k,t)$ is proportional to the fourth time derivative of $F_{11}^{(at)}(k,t)$, because of conservation law, so that the hydrogen term is multiplied by A_{RH}^2, which is of order 100, and becomes comparable ($\sim65\%$) to the amplitude corresponding to the oxygen motion. As a consequence, it produces the inflection at ~0.004 ps, visible in $F_{44}^{(at)}(k,t)$, Figs. 15(c) and 15(d).

IV. SUMMARY AND CONCLUSIONS

This study has mainly been devoted to the analysis of thermal conductivity λ of water at normal temperature and in the supercooled region, 255 K. The values obtained with the SPC/E model are in good agreement with the experimental data and do not depend on the formalism adopted, within the statistical uncertainty.

The most prominent feature of the energy flux CF is a large oscillation with characteristic frequencies typical of librational dynamics. The large value of $\lambda(\omega)$ in this frequency region may be essential in the very early stage of fundamental solvation processes. For instance, the asymmetric stretch of the OH bond and a libration have been shown [27] to be strongly involved in the absorption of the energy released by an excited electron that decays to its ground state.

The large high-frequency oscillation of the energy flux CF is a distinctive feature of water, compared, e.g., with that observed for *n*-butane [20] or, even more, the Lennard-Jones fluid. The former only shows a small oscillation centered at ~30 THz, while the LJ fluid has a monotonically decreasing energy flux CF [28].

The possibility of computing λ according to a molecular and an atomic definition has been exploited to show which dynamical modes of water most contribute to this transport parameter, at $k=0$. It turned out that two low-frequency exponential-like modes determine the value of λ. The first is faster, with a decay rate of the order of collision time (~0.03 ps) and gives a positive contribution to λ. The slower exponential, conversely, decreases λ to an extent that depends strongly on temperature ($\sim40\%$ at 255 K and almost negligibly at 300 K). The temperature dependence of this mode accounts for the anomalous behavior of thermal conductivity of water, that decreases as a function of temperature, in the temperature range explored. Contributions to λ from higher-frequency dynamics, i.e., cage mode and librations, have been ruled out contrasting their rather different behavior in the molecular and atomic results. This procedure of analysis of the modes contributing to λ becomes more difficult to implement as temperature increases because of the broadening and merging of the corresponding bands.

We recall that the SPC/E model employed is a rigid one and does not account for internal vibrations of water. However, from the point of view of this transport parameter, it seems likely that internal vibrations can be safely neglected, as we found for librations.

The extension of this analysis to finite k's has shown a decrease of λ as a function of k, with a smooth transition between the $k=0$ and the finite k values, analogous to that observed for generalized viscosities [2].

Generalized thermodynamic properties have been calculated as the second principal contribution of this work. We found that the initial values of the density-energy and energy-energy correlation functions, $F_{13}(k,t)$ and $F_{33}(k,t)$, when properly normalized, contain a collective part which is given by the structure factor of the liquid. The difference observed in the k dependence of the molecular and atomic values of $c_v(k)$, $h(k)$, $\alpha(k)$, and $\gamma(k)$ has been traced back to rotational terms typically in the frequency range around 45 THz, cage mode. On the other hand, the limit behavior of these functions for $k=0$ is independent of the molecular or atomic definition, while in the region up to ~5 Å^{-1} the potential and kinetic contribution to, e.g., $h(k)$ reflects the peak position of the partial structure functions, mainly for the OH and HH pairs.

The set of results presented extends the knowledge of the behavior of the SPC/E model of water to a number of col-

lective dynamical properties and to the supercooled region, allowing also a comparison with the corresponding results of the TIP4P potential. Overall, it appears that the SPC/E water model gives results in better agreement with experimental data than TIP4P. The extent of improvement varies from a property to another, being larger for, e.g., diffusion and dielectric properties and smaller for thermal conductivity. A feature shared by both models is the insufficient slowing down of the dynamics at low temperature, again more apparent for TIP4P than for SPC/E. This is manifested by the values of diffusion and viscosity in the supercooled region. Presumably, this is a consequence of an incorrect account of the temperature dependence of nonadditive interactions, which the enhanced dipole moments of the models only describe in an average way, with parameters optimized on properties at normal temperature.

Finally, we mention a very accurate MD study of thermal conductivity of Lennard-Jones fluid by Vogelsang, Hoheisel, and Ciccotti [29], where the effect of truncation of potential and averaging procedure on the results is examined. The results show a small number dependence, that, if extended to our data, would further improve the agreement with the experimental values. In addition, this study [29] proves that nonequilibrium [30] and equilibrium MD lead to values of thermal conductivity in quantitative agreement.

[1] D. Bertolini and A. Tani, Phys. Rev. E **51**, 1091 (1995).
[2] D. Bertolini and A. Tani, Phys. Rev. E **51**, 1699 (1995).
[3] W. L. Jorgensen, J. Chandrasekhar, J. D. Madura, R. W. Impey, and M. L. Klein, J. Chem. Phys. **79**, 926 (1983).
[4] H. J. C. Berendsen, J. R. Grigera, and T. P. Straatsma, J. Phys. Chem. **91**, 6269 (1987).
[5] I. M. de Schepper, E. G. D. Cohen, C. Bruin, J. C. van Rijis, W. Montfrooij, and L. A. de Graaf, Phys. Rev. A **38**, 271 (1988).
[6] J. P. Hansen and I. R. McDonald, *Theory of Simple Liquids* (Academic, London, 1986).
[7] P. Schofield, Proc. Phys. Soc. London **88**, 149 (1966); in *Physics of Simple Liquids*, edited by H. N. V. Temperley, J. S. Rowlinson, and G. S. Rushbrooke (North-Holland, Amsterdam, 1968).
[8] M. A. Ricci, D. Rocca, G. Ruocco, and R. Vallauri, Phys. Rev. A **40**, 7226 (1989).
[9] D. Bertolini and A. Tani, Mol. Phys. **75**, 1047 (1992); **75**, 1065 (1992).
[10] W. E. Alley and B. J. Alder, Phys. Rev. A **27**, 3158 (1983).
[11] G. Ciccotti, J. P. Ryckaert, and M. Ferrario, Mol. Phys. **47**, 1253 (1982).
[12] C. A. Angell, M. Oguni, and W. J. Sichina, J. Phys. Chem. **86**, 998 (1982).
[13] D. E. Hare and C. M. Sorensen, J. Chem. Phys. **87**, 4840 (1987).
[14] G. S. Kell, J. Chem. Eng. Data **12**, 66 (1967).
[15] C. A. Angell, in *Water, a Comprehensive Treatise*, edited by F. Franks (Plenum, New York, 1982), Vol. VII.
[16] D. Bertolini, M. Cassettari, and G. Salvetti, J. Chem. Phys. **76**, 3285 (1982).
[17] U. Kaatze and V. Uhlendorf, Z. Phys. Chem. Neue Folge **126**, 151 (1981).
[18] J. Teixeira and J. Leblond, J. Phys. (France) Lett. **39**, L83 (1978); O. Conde, J. Teixeira, and P. Papon, J. Chem. Phys. **76**, 3747 (1982).
[19] V. P. Isachenko, V. A. Osipova, and A. S. Sukomel, *Heat Transfer* (Mir, Moscow, 1980).
[20] G. Marechal and J. P. Ryckaert, Chem. Phys. Lett. **101**, 548 (1983).
[21] Y. Kataoka, Bull. Chem. Soc. Jpn. **62**, 1421 (1989).
[22] V. Carravetta and E. Clementi, J. Chem. Phys. **81**, 2646 (1984).
[23] B. J. Berne, J. P. Boone, and S. A. Rice, J. Chem. Phys. **45**, 1086 (1966).
[24] J. R. D. Copley and S. W. Lovesey, Rep. Prog. Phys. **38**, 461 (1975).
[25] A. K. Soper, J. Chem. Phys. **101**, 6888 (1994); A. K. Soper and M. G. Phillips, Chem. Phys. **107**, 47 (1986).
[26] W. L. Jorgensen and J. D. Madura, Mol. Phys. **56**, 1381 (1985); L. A. Báez and P. Clancy, J. Chem. Phys. **101**, 9837 (1994).
[27] O. V. Prezhdo and P. J. Rossky, J. Phys. Chem. **100**, 17 094 (1996).
[28] D. Levesque, L. Verlet, and J. Kurkijarvi, Phys. Rev. A **7**, 1690 (1973).
[29] R. Vogelsang, C. Hoheisel, and G. Ciccotti, J. Chem. Phys. **86**, 6371 (1987).
[30] D. J. Evans, Phys. Lett. **91A**, 457 (1982).